DOI: 10.1002/ejic.200801088

Solid-State and Solution Structure of Lanthanide(III) Complexes with a Flexible Py-N_6 Macrocyclic Ligand

Cristina Núñez,[a] Marta Mato-Iglesias,[b] Rufina Bastida,[a] Alejandro Macías,[a] Paulo Pérez-Lourido,[c] Carlos Platas-Iglesias,*[b] and Laura Valencia*[c]

Keywords: Lanthanides / Macrocyclic ligands / Density functional calculations / X-ray diffraction

Lanthanide complexes of a hexaaza macrocyclic ligand containing a pyridine head unit (L) were synthesized (Ln = La–Lu, except Pm). The solid-state structures of the corresponding La, Ce, Pr, Nd, and Lu complexes were determined by single-crystal X-ray crystallography, and they reveal the presence of three different mononuclear complexes with three different conformations of the macrocycle and coordination environments around the metal ions. In all complexes the lanthanide ion is coordinated in an endomacrocyclic manner to the six nitrogen donor atoms of the ligand. In the La, Ce, and Pr complexes the metal ions show a 12-coordinate mononuclear environment in which 3 nitrate anions coordinate in a bidentate fashion. However, in the Nd analogue the metal ion displays a 10-coordinated environment with the coordination of 2 bidentate nitrate groups, whereas Lu shows a 9-coordinate environment interacting with 2 nitrate ligands, one of them acting as bidentate and the second one coordinating in a monodentate fashion. The ^1H and ^{13}C NMR spectra of the complexes recorded in CD_3CN suggest that the complexes adopt in solution a similar structure to that observed for the Nd complex in the solid state. The $[Ln(L)(NO_3)_3]$ and $[Ln(L)(NO_3)_2]^+$ complexes were characterized by density functional theory (DFT) calculations (B3LYP model). The structures obtained from these calculations for La, Ce, Pr, and Nd are in good agreement with the experimental solid-state structures. The relative stabilities of the $[Ln(L)(NO_3)_2]^+$ complexes with respect to the $[Ln(L)(NO_3)_3]$ ones (Ln = La, Nd, Gd, Ho, or Lu) were studied both in vacuo and in acetonitrile solution (PCM model) at the same computational level. Our calculations indicate that in solution the $[Ln(L)(NO_3)_2]^+$ species is the most stable one along the whole lanthanide series, in agreement with the NMR spectroscopic data.

Introduction

Applications of trivalent lanthanide complexes as contrast agents for NMR imaging,[1] stains for fluorescence imaging,[2] responsive luminescent systems,[3] catalysts for specific cleavage of RNA hydrolysis,[4] or as active agents in cancer radiotherapy[5] have prompted considerable interest in lanthanide coordination chemistry.[6] Among the receptors used to encapsulate lanthanide(III) ions, macrocyclic platforms play an essential role,[7] as they often form thermodynamically stable and kinetically inert complexes. Functionalized aza macrocycles such as H_4DOTA (H_4DOTA = 1,4,7,10-tetraazacyclododecane-1,4,7,10-tetraacetic acid) and related compounds are the most thoroughly studied ligands of this kind. Pyridine-based macrocyclic ligands were also shown to bind efficiently Ln^{III} ions, 12-membered rings bearing acetate or phosphonate pendant arms to yield very stable complexes.[8] Moreover, 18-membered hexaaza macrocycles such as L^1 (Scheme 1) derived from the condensation of 2,6-pyridinedicarbaldehyde or 2,6-diacetylpyridine and diamines provide a relatively large cavity that allows efficient complexation of lanthanide(III) ions.[9] This macrocyclic platform may be easily functionalized with pendant arms containing additional donor atoms, which allows the cation binding ability of the parent hexaaza macrocycle to be enhanced.[10–12]

Herein we report the coordination ability of the hexaaza macrocyclic ligand L towards Ln^{III} ions (Scheme 1). This ligand is potentially hexadentate for the coordination of Ln^{III} ions and can be further functionalized with pendant arms that should enhance its cation binding affinity. The solid-state structures of the corresponding La^{III}, Ce^{III}, Pr^{III}, Nd^{III}, and Lu^{III} complexes were determined by single-crystal X-ray crystallography. The structure of the complexes in solution was investigated by NMR spectroscopic techniques in acetonitrile solution. Finally, the complexes were also characterized by density functional theory (DFT) calcula-

[a] Departamento de Química Inorgánica, Facultad de Química, Universidad de Santiago de Compostela,
Avda. de las Ciencias s/n, 15782 Santiago de Compostela, Spain
[b] Departamento Química Fundamental, Facultade de Ciencias, Universidade da Coruña,
Alejandro de la Sota 1, 15008 A Coruña, Spain
[c] Departamento de Química Inorgánica, Facultad de Ciencias, Universidade de Vigo,
As Lagoas, Marcosende, Pontevedra, Spain

Supporting information for this article is available on the WWW under http://www.eurjic.org or from the author.

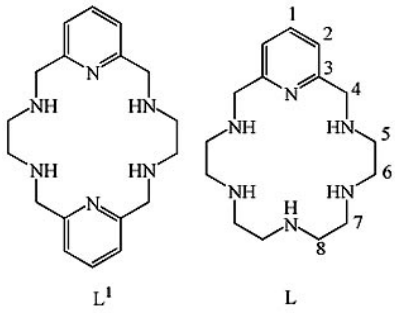

Scheme 1.

tions (B3LYP model). These calculations were used to rationalize the different structures of the complexes observed along the lanthanide series.

Results and Discussion

Synthesis and Characterization of the Complexes

Reaction of L (Scheme 1) with the appropriate hydrated lanthanide nitrate in acetonitrile led to mononuclear complexes of the formula $[M(L)](NO_3)_3 \cdot xCH_3CN \cdot yH_2O$ (M = La–Lu, except Pm) in good yields (44–87%). The ligand reacted quickly with Ln^{III} ions to produce kinetically stable complexes, which were characterized by elemental analysis, IR and NMR spectroscopy, and FAB MS. The IR spectra recorded as KBr discs show similar features for all compounds. The spectra feature split bands associated with ν(C=N) and ν(C=C) vibrations of the pyridine ring, which are shifted to higher wavenumbers by complexation due to the interaction between the metal ions and the pyridine nitrogen atom.[13] In all complexes, the band at 1383 cm^{-1} associated with the presence of ionic nitrate is accompanied by several bands that clearly identify the presence of coordinated nitrate groups.[14] The spectra also show several bands between 3200–3500 cm^{-1}, corresponding to the NH groups present in the molecule. The FAB mass spectrum of most compounds displays peaks corresponding to the $[LnL(NO_3)_2]^+$, $[LnL(NO_3)]^+$, or $[LnL]^+$ fragments, together with a peak at m/z = 293 corresponding to $[L + H]^+$, which confirms the formation of all the lanthanide complexes.

X-ray Crystal Structures

The solid-state structures of compounds **1**–**4** and **14** were determined by single-crystal X-ray diffraction analyses. The data set obtained for **14** had low quality; however, the results were sufficient to establish the overall geometry of the complex. Attempts to obtain single crystals suitable for X-ray diffraction analysis for the remaining compounds reported in this work were unsuccessful.

Compounds **1** and **2** crystallize in the triclinic space group $P\bar{1}$, whereas compounds **3**, **4**, and **14** crystallize in the monoclinic space groups $P2_1/n$ (**3** and **4**) and $P2_1/c$ (**14**). Crystals of **1**, **2**, and **3** contain the neutral complexes $[LnL(NO_3)_3]$ (Ln = La, Ce, or Pr), whereas in **4** and **14**, the asymmetric unit contains the cation $[LnL(NO_3)_2]^+$ (Ln = Nd or Lu) and a well-separated nitrate (**4**) or perchlorate (**14**) anion. The perchlorate anion in **14** comes from the ligand synthesis. Hydration water molecules are present in the crystal lattice of compounds **1**–**4**. Selected bond lengths of the lanthanide coordination environment in $[LnL(NO_3)_3]$ (Ln = La, Ce, or Pr) and $[LnL(NO_3)_2]^+$ (Ln = Nd or Lu) complexes are given in Table 1, whereas bond angles of the lanthanide coordination sphere are given as Supporting Information (Table S1). ORTEP plots of the different complexes present in the crystals of **1**, **4**, and **14** are shown in Figures 1, 2, and 3, respectively. The ORTEP plots of the Ce and Pr complexes, which are very similar to that of the La analogue, are given as Supporting Information (Figures S1 and S2).

Table 1. Experimental[a] and calculated[b] bond lengths [Å] of the metal coordination environment in $[Ln(L)(NO_3)_3]$ and $[Ln(L)(NO_3)_2]^+$ complexes (Ln = La, Ce, Pr, Nd, or Lu).

	$[La(L)(NO_3)_3]$		$[Ce(L)(NO_3)_3]$		$[Pr(L)(NO_3)_3]$		$[Nd(L)(NO_3)_2]^+$		$[Lu(L)(NO_3)_2]^+$	
	Exp.[a]	Calcd.[b]	Exp.[a]	Calcd.[b]	Exp.[a]	Calcd.[b]	Exp.[a]	Calcd.[b]	Exp.[a]	Calcd.[b]
Ln1–N1	2.7896(14)	2.895	2.7780(13)	2.885	2.804(2)	2.884	2.699(2)	2.734	2.41(3)	2.663
Ln1–N2	2.7628(15)	2.815	2.7426(13)	2.780	2.727(3)	2.789	2.707(2)	2.760	2.47(2)	2.661
Ln1–N3	2.8076(16)	2.849	2.7888(13)	2.840	2.763(3)	2.831	2.659(3)	2.746	2.47(4)	2.661
Ln1–N4	2.7707(15)	2.859	2.7536(13)	2.850	2.763(3)	2.842	2.650(2)	2.746	2.51(2)	2.647
Ln1–N5	2.7430(15)	2.812	2.7227(13)	2.798	2.743(3)	2.788	2.675(3)	2.746	2.49(2)	2.661
Ln1–N6	2.7988(15)	2.868	2.7848(13)	2.857	2.772(3)	2.852	2.689(2)	2.760	2.498(19)	2.661
Ln1–O1N	2.6882(13)	2.739	2.6491(11)	2.720	2.705(2)	2.703	2.526(2)	2.540	–	2.391
Ln1–O2N	2.7494(14)	2.734	2.7071(11)	2.711	2.681(2)	2.694	2.5208(19)	2.540	2.30(3)	2.391
Ln1–O4N	2.7872(14)	2.719	2.7426(11)	2.701	2.702(2)	2.686	2.572(2)	2.570	2.422(16)	2.432
Ln1–O5N	2.7661(14)	2.683	2.7343(11)	2.664	2.657(2)	2.647	2.557(2)	2.558	–	2.434
Ln1–O6N	–	–	–	–	–	–	–	–	2.36(2)	–
Ln1–O7N	2.7315(13)	2.698	2.6944(11)	2.681	2.718(2)	2.667	–	–	–	–
Ln1–O8N	2.7478(13)	2.698	2.7178(11)	2.681	2.721(2)	2.667	–	–	–	–
AF_i[c]	–	0.0236	–	0.0233	–	0.0199	–	0.0214	–	[d]

[a] From single-crystal X-ray diffraction analyses. [b] From DFT calculations at the B3LYP/6-31G(d) level. [c] $AF_i = [\Sigma(\text{exp.} - \text{calcd.})^2/\Sigma(\text{exp.})^2]^{1/2}$, where exp. and calcd. denote experimental and calculated values, respectively. [d] The minimum energy conformation obtained from DFT calculations is different to that observed in the solid state, and therefore, an agreement factor is not provided.

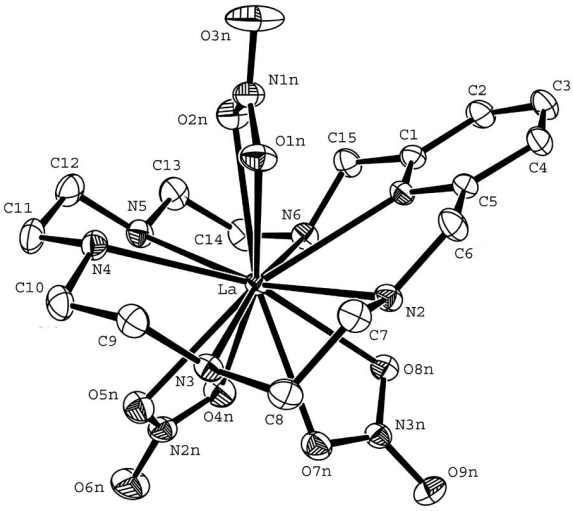

Figure 1. X-ray crystal structure of $[La(L)(NO_3)_3]$ showing the atomic numbering scheme. Hydrogen atoms are omitted for simplicity. The ORTEP plot is at the 30% probability level.

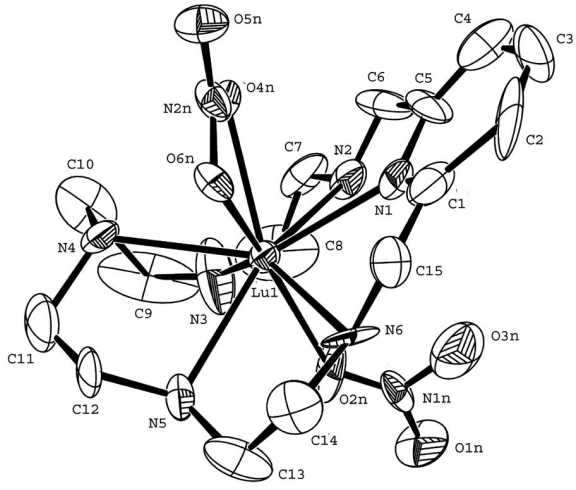

Figure 3. X-ray crystal structure of $[Lu(L)(NO_3)_2]^+$ showing the atomic numbering scheme. Hydrogen atoms are omitted for simplicity. The ORTEP plot is at the 30% probability level.

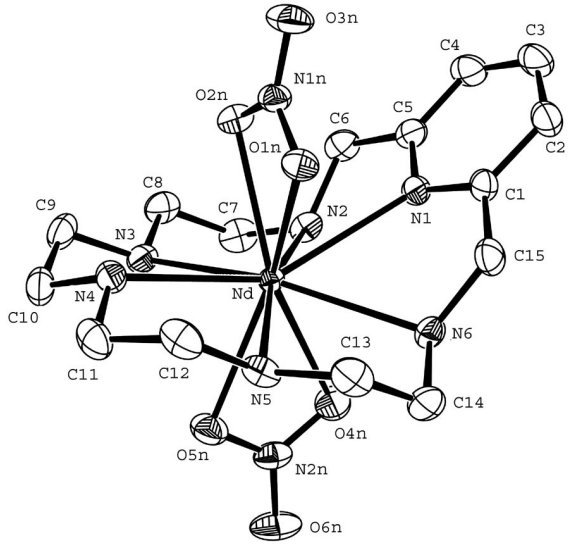

Figure 2. X-ray crystal structure of $[Nd(L)(NO_3)_2]^+$ showing the atomic numbering scheme. Hydrogen atoms are omitted for simplicity. The ORTEP plot is at the 30% probability level.

Inspection of the five X-ray structures of the lanthanide complexes reveals the presence of three different mononuclear complexes with three different conformations of the macrocycle and coordination environments around the metal ions. In all complexes, the lanthanide ion is coordinated in an endomacrocyclic manner. In **1**, **2**, and **3**, the metal ions show a 12-coordinate mononuclear environment, and they are bound to the 6 nitrogen donor atoms of the ligand and 6 oxygen atoms of 3 nitrate anions coordinated in a bidentate fashion. The neodymium ion in crystals of **4** displays a 10-coordinated environment and the metal ion is bonded to the 6 nitrogen atoms of the ligand and 2 bidentate nitrate groups. In **4**, one of the nitrate groups is not coordinated to the metal ion. In **14**, the Lu^{III} ion shows a nine-coordinate environment interacting with all nitrogen atoms of the macrocycle and with two nitrate ions; one of nitrate ions coordinates in a bidentate fashion, whereas the second coordinates in a monodentate fashion. A similar decrease in the coordination number along the lanthanide series was previously observed for other lanthanide complexes as a consequence of the lanthanide contraction.[10] The Ln–N and Ln–O bond lengths of the metal coordination environment are shorter in the Ce^{III} complex than in the La^{III} one. This is expected, as usually a progressive decrease in the Ln–donor atom bond lengths is observed upon decreasing the ionic radii of the lanthanide ion.[15] However, many of the Ln–N and Ln–O bond lengths are longer in the Pr^{III} complex than in the Ce^{III} one (N1, N4, N5, O1n, O7n, O8n), as previously observed for lanthanide complexes with a macrocyclic ligand.[16] These results are indicative of increasing steric crowding around the lanthanide ion for a 12-coordinate environment and anticipate the structural change observed along the lanthanide series between Pr and Nd. The La–N1 and Nd–N1 bond lengths are slightly longer than those observed for lanthanide complexes with an 18-membered Schiff base macrocyclic ligand containing pyridine head units.[17,18] In these complexes, the lanthanide ion shows the same coordination number as the corresponding complexes of L (in the La^{III} complex the metal ion is 12-coordinated, whereas in the corresponding Nd^{III} complex the metal ion is 10-coordinated). The La–O bond lengths in **1** are similar to those observed for other 12-coordinated complexes with NO_3^- ligands, but slightly longer than those observed for a 10-coordinate La^{III} texaphyrin with 2 coordinated nitrate ligands.[19]

In compounds **1**, **2**, and **3**, two of the bidentate nitrate ions are placed on one side of the macrocycle, which is folded to the third nitrate ion placed on the opposite side (Figure 1). In **4** and **14**, the two coordinated nitrate ions are placed on different sides of the macrocycle, and the ligand is V folded. The dihedral angle between the plane containing the N1N2N6 nitrogen atoms and the plane containing

the secondary amine atoms N3N4N5 in all complexes varies from 69.14° in **14** to 87.93° in **2**.

In the complexes each of the four ethylenediamine units forms a five-membered chelate ring that can adopt δ or λ conformations.[20] Attending to the conformation of the four five-membered chelate rings, three different isomers are found along the lanthanide series. In **1**, **2**, and **3**, the conformations of the chelate rings are identical and compounds $[Ln(L)(NO_3)_3]$ (Ln = La, Ce, Pr) present a λδλλ (or δλδδ) conformation. In **4**, the conformation is λδλδ, whereas in **14** a δλλλ conformation is observed. Attending to the configuration of the four chiral amine nitrogen atoms, all complexes present the same configuration [N2N3N5N6 show *SSRR* or *RRSS* configurations, as both enantiomers are present in the crystal].

For **1**, **2**, and **3**, the coordination polyhedron around the Ln^{III} ion can be described as an icosahedron (Figure 4a). In **4**, the donor atoms occupy the vertex of a hexagonal bipyramid, where the six nitrogen atoms of the ligand form the hexagonal plane and each of the axial positions are occupied by the bidentate nitrate groups (Figure 4b). In **14**, the polyhedron around the metal ion can be described as a distorted monocapped square antiprism that can be considered to comprise two pseudoparallel planes formed by N2–N3–N5–N6 and N1–N4–O4n–O6n, whereas O2n is capping the square face N2–N3–N5–N6. The main distortion from a regular square antiprism geometry is attributable to the small bite of the bidentate nitrate ligand.

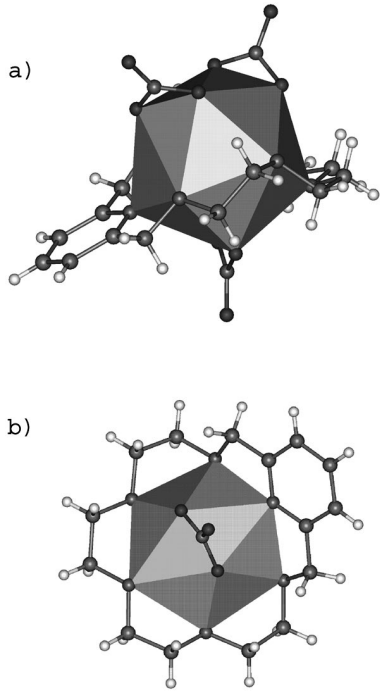

Figure 4. Coordination polyhedron of complexes $[La(L)(NO_3)_3]$ (a) and $[Nd(L)(NO_3)_2]^+$ (b).

Inspection of the crystal structures obtained reveals that face-to-face π–π interactions are established between pyridine rings in all complexes.[21] All complexes have similar arrangements in the crystal lattice. The ligand molecules are stacked by pairs and the pyridine rings lie parallel with interplanar distances of ca. 3.38 Å, whereas the distance between centroids is ca. 3.80 Å. The solid-state structures of compounds **1**–**4** and **14** indicate the presence of hydrogen-bonding interactions involving the hydrogen atoms of the water molecule, the ionic perchlorate or nitrate anions and the secondary amine nitrogen atoms of the ligand. Relevant hydrogen bonding data are given in Table S2 (Supporting Information).

NMR Spectra

The NMR spectra of the Ln^{III} complexes of L were recorded in CD_3CN solution at 298 K (Table 2). The proton spectrum of the diamagnetic La^{III} complex (Figure 5) shows the expected triplet and doublet signals due to the proton nuclei of the pyridine units at 7.77 and 7.24 ppm and two signals at 4.23 and 3.93 ppm attributable to the geminal H4 protons (see Scheme 1 for labeling). The signals due to protons H5–H8 are observed as overlapping multiplets between 2.4 and 3.2 ppm (Figure 5). The proton spectrum is consistent with an effective C_s or C_2 symmetry of the complex in solution. This is confirmed by the ^{13}C NMR spectrum, which shows 8 signals for the 15 carbon nuclei of the ligand backbone. The assignment of the ^1H NMR signals was achieved with the aid of standard COSY and HMQC 2D experiments (Table 2). The chemical shifts given in Table 2 for the H5–H8 protons were obtained from the cross-peaks observed in the HMQC spectrum. Although the specific CH_2 proton assignments of the axial and equatorial H4–H8 protons were not possible on the basis of the 2D NMR spectra, they were carried out by using the stereochemically dependent proton shift effects, resulting from the polarization of the C–H bonds by the electric field effect caused by the cation charge.[22] This results in deshielding of the equatorial protons that point away from the Ln^{III} ion.

Table 2. ^1H and ^{13}C NMR shifts (ppm with respect to TMS) for Ln^{III} complexes of L (see Scheme 1 for labeling).

^1H	La[a]	Ce[b]	Pr[b]	^{13}C	La[a]
H1	7.77	8.23	9.24	C1	139.9
H2	7.24	7.98	10.32	C2	122.0
$H4_{ax}$	3.93	7.60	14.23	C3	160.1
$H4_{eq}$	4.23	8.68	20.04	C4	55.3
$H5_{ax}$	2.77	9.79	17.91	C5	48.9
$H5_{eq}$	2.95	10.46	22.75	C6	51.1
$H6_{ax}$	2.77	12.01	25.11	C7	49.7
$H6_{eq}$	2.92	12.10	25.65	C8	50.1
$H7_{ax}$	2.74	5.33	10.30		
$H7_{eq}$	3.06	9.06	20.41		
$H8_{ax}$	2.56	4.79	13.95		
$H8_{eq}$	2.90	5.82	14.55		

[a] Assignment supported by 2D COSY and HMQC experiments at 298 K. [b] Assignment supported by 2D COSY experiments at 298 K.

The binding of a ligand to a paramagnetic Ln^{III} ion generally results in large NMR frequency shifts at the ligand nuclei, with magnitudes and signs depending on both the

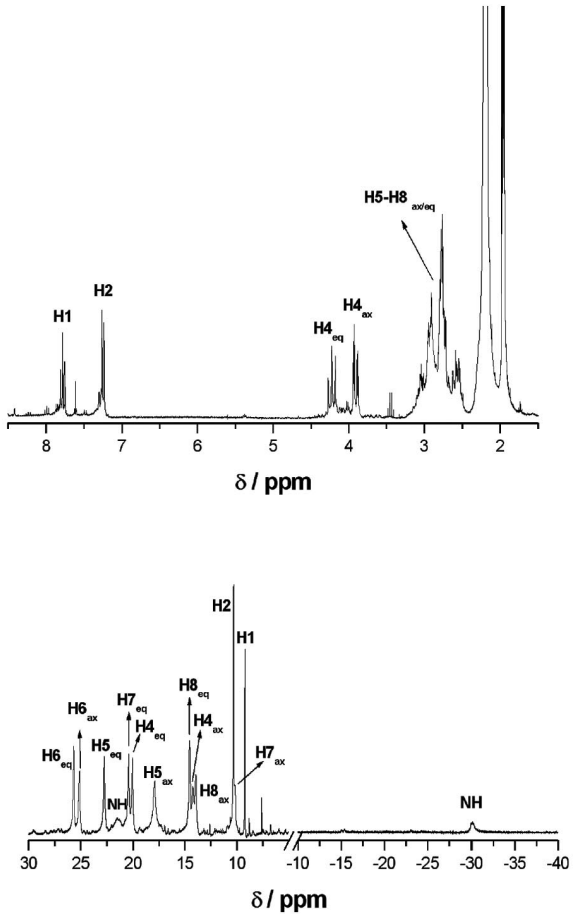

Figure 5. The ^{1}H NMR spectra of the La^{III} (top) and Pr^{III} (bottom) complexes of L as recorded in CD_3CN solution at 298 K.

nature of the lanthanide ion and the location of the nucleus relative to the metal center.[23] The ^{1}H NMR spectra of the paramagnetic Ce^{III} and Pr^{III} complexes show 12 signals (excluding those due to the NH protons), which again is in agreement with an effective C_s (or C_2) symmetry of the complexes in solution. The ^{1}H NMR signals indeed experience important paramagnetic shifts, as it can be seen by comparing the chemical shifts observed for the Ce^{III} and Pr^{III} complexes with those observed for the La^{III} analogue (Table 2). The assignments of the proton signals were based on standard 2D homonuclear COSY experiments, which gave strong cross-peaks between the geminal CH_2 protons (4–8) and between the *ortho*-coupled pyridyl protons. The 10 ^{1}H NMR peaks due to protons 4–8 can be grouped into two different sets according to their relative line broadening: 5 resonances are appreciably sharper than the remaining ones (Figure 5). These two sets of signals correspond to two sets of Ln^{III}–proton distances; the broader resonances are associated with the protons closer to the metal ion.[24] Thus, the broader resonances were assigned to axial protons, whereas the second set of signals was assigned to equatorial ones. A full assignment of the proton signals observed for the Ce^{III} and Pr^{III} complexes was achieved with the aid of the SHIFT ANALYSIS program developed by Forsberg.[25]

Inspection of the solid-state structures of the La^{III}, Ce^{III}, and Pr^{III} complexes described above indicates that these species present C_1 symmetry in the solid state, whereas the Nd^{III} complex shows a slightly distorted C_s symmetry, where the symmetry plane contains the Nd^{III} ion and the donor atoms of the macrocycle N1 and N4. The ^{1}H NMR spectra of the La^{III}, Ce^{III}, and Pr^{III} complexes are consistent with a relatively rigid C_s symmetry in solution. Indeed, the axial and equatorial protons give different signals in the proton spectrum, indicating that the $\lambda \rightarrow \delta$ interconversion processes of the five-membered chelate rings formed due to the coordination of the ligand are slow on the NMR timescale. Interestingly, the ^{1}H NMR spectra of the Nd^{III} and Eu^{III} complexes show similar features, but a full assignment of the signals was not possible. Thus, the Ln^{III} complexes of L appear to adopt a similar structure in solution to that observed for the Nd^{III} complex in the solid state, rather than that observed in the solid-state structures of the La^{III}, Ce^{III}, and Pr^{III} analogues.

DFT Calculations

The $[Ln(L)(NO_3)_3]$ and $[Ln(L)(NO_3)_2]^+$ systems (Ln = La, Ce, Pr, Nd, Gd, Ho, or Lu) were investigated by DFT calculations (B3LYP model). The quasirelativistic effective core potential (ECP) of Dolg et al. and the related [5s4p3d]–GTO valence basis set was applied in these calculations.[26] This ECP includes 46+4f^n electrons in the core, leaving the outermost 11 electrons to be treated explicitly, and this has provide reliable results for several lanthanide complexes with both macrocyclic[27,28] or acyclic[29–31] ligands. Relative to all-electron basis sets, ECPs account to some extent for relativistic effects, which are believed to become important for the elements from the fourth row of the periodic table.

The calculated geometries for the $[Ln(L)(NO_3)_3]$ (Ln = La, Ce, or Pr) and $[Ln(L)(NO_3)_2]^+$ (Ln = Nd or Lu) are compared in Table 1 with the experimental structures obtained from X-ray crystal-structure studies. The calculated bond lengths of the metal coordination environments in $[Ln(L)(NO_3)_3]$ complexes (Ln = La, Ce, or Pr) show reasonably good agreement with the solid-state data, as evidenced by the agreement factor obtained: AF_i = 0.0236, 0.0233, and 0.0199 for La, Ce, and Pr, respectively ($AF_i = [\Sigma(\text{exp.} - \text{calcd.})^2/\Sigma(\text{exp.})^2]^{1/2}$, where exp. and calcd. denote calculated and experimental values, respectively).[32] A similar agreement factor was also obtained for the $[Nd(L)(NO_3)_2]^+$ system (AF_i = 0.0214). The Ln–N bond lengths calculated for the $[Ln(L)(NO_3)_3]$ (Ln = La, Ce, or Pr) and $[Nd(L)(NO_3)_2]^+$ systems are ca. 0.04–0.10 Å longer than those observed experimentally, whereas the Ln–O bond lengths are in very good agreement with the solid-state data. An overestimation of the Ln–N distances in comparison to X-ray diffraction data is often observed when Ln^{III} complexes are studied in vacuo by HF or B3LYP calculations.[11,28]

In contrast to the La, Ce, Pr, and Nd analogues, the calculated geometry for the $[Lu(L)(NO_3)_2]^+$ system is quite dif-

ferent from the experimental X-ray structure. Indeed, geometry optimizations led systematically to a 10-coordinate complex, with both nitrate ligands coordinating in a bidentate fashion. Moreover, our calculations predict the λδλδ conformation (that observed for the Nd^{III} analogue) to be more stable than that observed in the solid state by 5.58 kcal mol^{-1}. This might be related to the ever-present issue that the lowest energy conformation for an isolated molecule may not be the one present in the crystal even at low temperature due to the fact that crystal forces may favor a higher energy conformation. In this case, an isolated molecule calculation of relative conformational energies will not provide an accurate prediction of the solid-state conformation. Thus, the structure that a molecule adopts in its crystalline form may differ significantly from that in the gas phase or in solution.

In view of the structural change observed for the complexes of L along the lanthanide series, the relative stabilities of the $[Ln(L)(NO_3)_2]^+$ complexes with respect to the $[Ln(L)(NO_3)_3]$ ones (Ln = La, Nd, Gd, Ho, or Lu) were determined in vacuo at the B3LYP/6-31G(d) level of theory by calculating the free energy variation for the reaction [Equation (1)] by:

$$[Ln(L)(NO_3)_2]^+ + NO_3^- \leftrightarrows [Ln(L)(NO_3)_3] \quad (1)$$

The gas-phase energies, enthalpies, and free energies for the reaction depicted in Equation (1) are provided in Table 3. In vacuo, the main difference along the lanthanide series lies in the variation in the electronic energy associated to Equation (1), whereas the nonpotential energy contributions (that is, zero-point energy and thermal terms) to ΔG_{298} do not change much along the lanthanide series. All ΔE_{elec} values are negative, but La presents the most favorable interaction energy (–106.0 kcal mol^{-1}). The overall free-energy variations have negative values in vacuo, and the values range from –88.8 kcal mol^{-1} for La^{III} to –73.5 kcal mol^{-1} for Lu^{III}. This highlights the tendency of the third NO_3^- anion to coordinate to the metal ions in vacuo, and this reaction becomes more favorable as the ionic radius of the Ln^{III} ion increases. These results contrast the experimental solid-state structures, which indicate a structural change along the Ln^{III} series: the lighter lanthanide ions (Ln = La–Pr) show a $[Ln(L)(NO_3)_3]$ structure, whereas the $[Ln(L)(NO_3)_2]^+$ complexes are observed in the solid state for Ln = Nd–Lu).

The ^1H and ^{13}C NMR spectra of the complexes of L were obtained from acetonitrile solutions of the isolated solids. Thus, in order to evaluate the solvent effects on the structure of the complexes, the relative stabilities of the $[Ln(L)(NO_3)_2]^+$ complexes with respect to the $[Ln(L)(NO_3)_3]$ ones were also calculated in acetonitrile. In these calculations the effect of the bulk solvent was included by using the polarizable continuum model (PCM). The main results are given in Table 3. Our results show that the inclusion of solvent effects dramatically affects the free energies for Equation (1) as a consequence of the large and positive solvation free energies (ΔG_{sol}). The data reported in Table 3 also show that the inclusion of nonelectrostatic contributions provokes a minor effect on the calculated ΔG_{sol} values. The large positive ΔG_{sol} values obtained for this reaction are indeed expected,[33] as solvation stabilizes a charged solute by polarization of the polar solvent. The effect is proportional to the charge squared and inversely proportional to the distance between charge and polarizable medium. Thus, solvation strongly stabilizes the left-hand side of Equation (1) as a result of the strong stabilization of the compact NO_3^- anion due to the shorter distance between the charge and the polarizable medium. This simple picture also explains why the ΔG_{sol} values are fairly constant along the lanthanide series. The free-energy variations have positive values in acetonitrile ranging from 0.19 kcal mol^{-1} for La^{III} to 12.59 kcal mol^{-1} for Lu^{III}. Thus, the calculated ΔG_{react} values indicate that the $[Ln(L)(NO_3)_2]^+$ species is the most stable one along the whole lanthanide series in acetonitrile solution, in nice agreement with the experimental NMR spectroscopic data.

Table 3. Gas-phase energies, enthalpies, and free energies, solvation energy contributions, and free energy of reaction in solution [kcal mol^{-1}] for Equation (1) at the B3LYP/6-31 G(d) level.[a]

	La	Nd	Gd	Ho	Lu
ΔE_{elec}	–106.03	–101.97	–97.02	–92.87	–88.61
ΔZPE	1.49	1.44	1.40	1.31	1.10
ΔE_0	–104.54	–100.53	–95.62	–91.56	–87.51
ΔE_{298}	–102.54	–98.52	–93.59	–89.57	–85.64
ΔH_{298}	–103.13	–99.11	–94.19	–90.16	–86.23
ΔG_{298}	–88.76	–85.15	–80.66	–76.95	–73.51
ΔG_{sol}[b]	86.42	86.73	86.75	86.79	86.79
ΔG_{sol}[c]	88.95	86.99	86.74	86.72	86.10
ΔG_{react}[d]	0.19	1.84	6.08	9.77	12.59

[a] Each contribution to ΔG_{react} is calculated according to $\Delta X = X([Ln(L)(NO_3)_3]) - X([Ln(L)(NO_3)_2]^+ - X(NO_3^-)$. [b] Solvation free energy including only electrostatic contribution. [c] Solvation free energy including both electrostatic and nonelectrostatic contributions. [d] Free energy of reaction in solution including both electrostatic and nonelectrostatic contributions.

Conclusions

The structure of the lanthanide complexes of the PyN_6 macrocyclic ligand (L) was investigated by using both experimental and theoretical tools. The X-ray crystal structures of the La, Ce, Pr, Nd, and Lu complexes show hexadentate binding of the ligand to all lanthanide ions. However, these series of compounds adopt at least three different structures in the solid state along the lanthanide series: (i) In the La, Ce, and Pr complexes, the metal ions show a 12-coordinate environment in which 3 nitrate anions coordinate in a bidentate fashion. (ii) In the Nd complex, the metal ion shows a 10-coordinate environment due to the coordination of 2 nitrate ligands in a bidentate fashion. (iii) In the Lu complex, the metal ion shows a 9-coordinate environment due to the coordination of a bidentate nitrate ligand and a monodentate one. By contrast, NMR spectroscopic studies performed in acetonitrile solution suggest that in solution only two NO_3^- ligands are coordinated to the metal ion even for the largest lanthanides (La–Pr). This

result has been confirmed by using DFT calculations, which predict that the $[Ln(L)(NO_3)_2]^+$ species is more stable than the $[Ln(L)(NO_3)_3]$ one along the whole lanthanide series from La to Lu. Most likely the neutral complexes $[Ln(L)(NO_3)_3]$ are isolated in the solid state due to their low solubility in a relatively polar solvent such as acetonitrile. The results reported in this work indicate that the macrocyclic cavity of L is well suited for the coordination of lanthanide ions. We are currently investigating ways to introduce different pendant arms into the framework of L to prepare stable lanthanide complexes in aqueous solution.

Experimental Section

Measurements: Elemental analyses were performed with a Carlo–Erba EA microanalyzer. IR spectra were recorded as KBr discs with a Bruker IFS-66V instrument. LSI mass spectra were recorded by using a Micromass Autospec spectrometer with 3-nitrobenzyl alcohol as the matrix. ^1H, ^{13}C, COSY, and HMQC NMR spectra were recorded in CD_3CN solutions with a Bruker AMX 500 NMR spectrometer operating at 499.80 MHz.

Materials: 2,6-Pyridinedicarbaldehyde was prepared according to a literature procedure.[34] Tetraethylenepentaamine and hydrated lanthanide(III) nitrates were obtained from Aldrich. All solvents used were of reagent grade and purified by usual methods.

L: The ligand was prepared by a modification of the method of Rothermel et al.[35] A solution of tetraethylenepentaamine (0.946 g, 5 mmol) in anhydrous methanol (25 mL) was added dropwise to a stirred solution of 2,6-pyridinedicarbaldehyde (0.675 g, 5 mmol) and $Ba(ClO_4)_2$ (1.6812 g, 5 mmol) in anhydrous methanol (250 mL). The mixture was heated at reflux for 4 h and then left to cool. $NaBH_4$ (0.60 g, 15 mmol) was added slowly in small portions, the flask was placed in an ice bath, and the mixture was stirred for 30 min. A second addition of $NaBH_4$ (0.30 g, 7.5 mmol) was made in small portions, and the resulting solution was stirred at room temperature for 2 h. The solvent was evaporated, and the residue was then extracted with chloroform (4 × 50 mL). The organic layer was dried with $MgSO_4$, filtered, and the solvent was evaporated to dryness. The resulting yellow oil was recrystallized from methanol to yield a white crystalline product. The solid was dissolved in water (150 mL) and H_2SO_4 was added dropwise until acid pH. The white precipitate was filtered off and NH_3 was added to the solution until pH 11. The solution was extracted with chloroform (4 × 50 mL). The organic layer was dried with $MgSO_4$, filtered, and the solvent was evaporated to dryness to yield a brown oil characterized as L. Yield: 0.968 g, 59%. M.p. 120 °C. ^1H NMR (300 MHz, $CDCl_3$, 25 °C): δ = 7.56 (t, 1 H, *py*), 7.05 (d, 2 H, *py*), 3.94 (s, 4H py-CH_2-NH), 2.85–3.05 (m, 16 H, CH_2-CH_2), 2.68 (b, 5 H, *NH*) ppm. ^{13}C NMR (75 MHz, $CDCl_3$, 25 °C): δ = 136.64 (*py*), 120.83 (*py*), 158.80 (*py*), 54.90 (CH_2-NH), 49.20, 49.09 and 48.97 (CH_2-CH_2) ppm. MS (FAB): *m*/*z* = 293 $[L + H]^+$. IR (KBr): $\tilde{\nu}$ = 1591 (m), 1457 (m), [ν(C=N)$_{py}$, ν(C=C)$_{py}$], 3316 (m), [ν(NH)] cm^{-1}. $C_{15}H_{28}N_6{\cdot}2H_2O$ (328.45): calcd. C 54.9, H 9.8, N 25.6; found C 54.8, H 9.9, N 25.9.

General Procedure for the Preparation of the Complexes: A solution of $Ln(NO_3)_3{\cdot}xH_2O$ (0.1 mmol) in acetonitrile (2 mL) was added to a stirred solution of L (0.029 g, 0.1 mmol) in acetonitrile (3 mL). The solution was stirred for 2 h at room temperature. The precipitate formed was isolated by filtration.

$[La(L)](NO_3)_3{\cdot}4H_2O$ (1): Yield: 0.030 g (44%). MS (FAB): *m*/*z* = 555 $[LaL(NO_3)_2]^+$. IR (KBr): $\tilde{\nu}$ = 1602 (m), 1452 (m) [ν(C=C) and ν(C=N)$_{py}$], 1452 (s), 1384 (s), 1304 (s), 1101 (s) [$\nu(NO_3^-)$], 3260 (m), 3297 (m), 3507 (m), 3579 (m) [ν(NH)] cm^{-1}. $C_{15}H_{36}LaN_9O_{13}$ (689.40): calcd. C 26.1, H 5.3, N 18.3; found C 25.9, H 5.4, N 18.6. Crystals of formula $[La(L)(NO_3)_3]{\cdot}H_2O$ suitable for X-ray diffraction were grown from an acetonitrile solution of the isolated solid.

$[Ce(L)](NO_3)_3{\cdot}5H_2O$ (2): Yield: 0.031 g (44%). ^{13}C NMR (75 MHz, CD_3CN, 50 °C): δ = 159.6, 140.0, 125.8, 58.0, 57.4, 56.1, 50.2, 49.0 ppm. MS (FAB): *m*/*z* = 556 $[CeL(NO_3)_2]^+$. IR (KBr): $\tilde{\nu}$ = 1604 (w) [ν(C=C) and ν(C=N)$_{py}$], 1487 (s), 1384 (s), 1307 (s), 1087 (s) [$\nu(NO_3^-)$], 3271 (m) [$\nu(NO_3^-)$] cm^{-1}. $C_{15}H_{38}CeN_9O_{14}$ (708.63): calcd. C 25.4, H 5.4, N 17.7; found C 25.2, H 5.2, N 18.1. Crystals of formula $[Ce(L)(NO_3)_3]{\cdot}H_2O$ suitable for X-ray diffraction were grown from an acetonitrile solution of the isolated solid.

$[Pr(L)](NO_3)_3{\cdot}H_2O$ (3): Yield: 0.039 g (57%). ^{13}C NMR (75 MHz, CD_3CN, 50 °C): δ = 165.1, 140.3, 133.0, 65.8, 63.0, 62.3, 53.4, 50.2 ppm. MS (FAB): *m*/*z* = 557 $[PrL(NO_3)_2]^+$, 495 $[PrL(NO_3)]^+$, 293 $[L + H]^+$. IR (KBr): $\tilde{\nu}$ = 1602 (m) [ν(C=C) and ν(C=N)$_{py}$], 1491 (s), 1384 (s), 1302 (s), 1091 (s) [$\nu(NO_3^-)$], 3210 (m) [ν(NH)] cm^{-1}. $C_{15}H_{30}N_9O_{10}Pr$ (637.36): calcd. C 28.3, H 4.8, N 19.8; found C 28.4, H 4.5, N 20.0. Crystals of formula $[Pr(L)(NO_3)_3]$ suitable for X-ray diffraction were grown from an acetonitrile solution of the isolated solid.

$[Nd(L)](NO_3)_3{\cdot}H_2O$ (4): Yield: 0.044 g (69%). MS (FAB): *m*/*z* = 558 $[NdL(NO_3)_2]^+$, 496 $[NdL(NO_3)]^+$, 293 $[L + H]^+$. IR (KBr): $\tilde{\nu}$ = 1601 [ν(C=C) and ν(C=N)$_{py}$], 1499 (s), 1384 (s), 1277 (s), 1093 (s) [$\nu(NO_3^-)$], 3305 (m), 3253 (m), 3231 (m), 3204 (s) [ν(NH)] cm^{-1}. $C_{15}H_{30}N_9NdO_{10}$ (640.69): calcd. C 28.1, H 4.7, N 19.7; found C 28.0, H 4.7, N 19.4. Crystals of formula $[Nd(L)(NO_3)_2](NO_3){\cdot}H_2O$ suitable for X-ray diffraction were grown from an acetonitrile solution of the isolated solid.

$[Sm(L)](NO_3)_3{\cdot}H_2O$ (5): Yield: 0.041 g (64%). MS (FAB): *m*/*z* = 568 $[SmL(NO_3)_2]^+$, 293 $[L + H]^+$. IR (KBr): $\tilde{\nu}$ = 1604 (m) [ν(C=C) and ν(C=N)$_{py}$], 1505 (s), 1384 (s), 1278 (s), 1057 (s) [$\nu(NO_3^-)$], 3210 (m) [ν(NH)] cm^{-1}. $C_{15}H_{30}N_9O_{10}Sm$ (646.81): calcd. C 27.8, H 4.6, N 19.5; found C 27.7, H 4.4, N 19.0.

$[Eu(L)](NO_3)_3{\cdot}2H_2O$ (6): Yield: 0.050 g (75%). MS (FAB): *m*/*z* = 569 $[EuL(NO_3)_2]^+$, 507 $[EuL(NO_3)]^+$, 446 $[EuL]^+$, 293 $[L + H]^+$. IR (KBr): $\tilde{\nu}$ = 1606 (m) [ν(C=C) and ν(C=N)$_{py}$], 1498 (s), 1384 (s), 1308 (s), 1029 (s) [$\nu(NO_3^-)$], 3267 (m) [ν(NH)] cm^{-1}. $C_{15}H_{32}EuN_9O_{11}$ (666.43): calcd. C 27.0, H 4.8, N 18.9; found C 27.4, H 4.6, N 18.8.

$[Gd(L)](NO_3)_3{\cdot}6H_2O$ (7): Yield: 0.033 g (44%). MS (FAB): *m*/*z* = 574, $[GdL(NO_3)_2]^+$, 512 $[GdL(NO_3)]^+$, 293 $[L + H]^+$. IR (KBr): $\tilde{\nu}$ = 1608 (m) [ν(C=C) and ν(C=N)$_{py}$], 1491 (s), 1384 (s), 1316 (s), 1031 (s) [$\nu(NO_3^-)$], 3281 (m) [ν(NH)] cm^{-1}. $C_{15}H_{40}GdN_9O_{15}$ (743.78): calcd. C 24.2, H 5.4, N 16.9; found C 24.3, H 5.5, N 16.7.

$[Tb(L)](NO_3)_3{\cdot}4H_2O$ (8): Yield: 0.031 g (43%). MS (FAB): *m*/*z* = 575 $[TbL(NO_3)_2]^+$, 513 $[TbL(NO_3)]^+$, 293 $[L + H]^+$. IR (KBr): $\tilde{\nu}$ = 1606 (m) [ν(C=C) and ν(C=N)$_{py}$], 1502 (s), 1384 (s), 1288 (s), 1030 (s) [$\nu(NO_3^-)$], 3283 (m), 3207 (m) [ν(NH)] cm^{-1}. $C_{15}H_{36}N_9O_{13}Tb$ (709.42): calcd. C 25.4, H 5.1, N 17.8; found C 25.7, H 5.0, N 17.9.

$[Dy(L)](NO_3)_3{\cdot}2H_2O$ (9): Yield: 0.033 g (48%). MS (FAB): *m*/*z* = 580 $[DyL(NO_3)_2]^+$, 518 $[DyL(NO_3)]^+$, 456 $[DyL]^+$, 293 $[L + H]^+$. IR (KBr): $\tilde{\nu}$ = 1607 (m) [ν(C=C) and ν(C=N)$_{py}$], 1505 (s), 1384 (s), 1283 (s), 1030 (s) [$\nu(NO_3^-)$], 3193 (m) [ν(NH)] cm^{-1}. $C_{15}H_{32}DyN_9O_{11}$ (678.15): calcd. C 26.6, H 4.8, N 18.6; found C 26.8, H 4.7, N 18.8.

$[Ho(L)](NO_3)_3{\cdot}2H_2O{\cdot}3CH_3CN$ (10): Yield: 0.055 g (68%). MS (FAB): *m*/*z* = 581 $[HoL(NO_3)_2]^+$, 519 $[HoL(NO_3)]^+$, 293 $[L + H]^+$. IR (KBr): $\tilde{\nu}$ = 1604 (m) [ν(C=C) and ν(C=N)$_{py}$], 1501 (s), 1384 (s),

1010 (s) [ν(NO_3^-)], 3182 (m), 3271 (m) [ν(NH)] cm^{-1}. $C_{21}H_{41}HoN_{12}O_{11}$ (802.55): calcd. C 31.4, H 5.1, N 20.9; found C 31.4, H 5.4, N 20.6.

[Er(L)](NO$_3$)$_3$·4H$_2$O (11): Yield: 0.42 g (59%). MS (FAB): *m*/*z* = 582 $[ErL(NO_3)_2]^+$, 520 $[ErL(NO_3)]^+$, 293 $[L + H]^+$. IR (KBr): $\tilde{\nu}$ = 1606 (m) [ν(C=C) and ν(C=N)$_{py}$], 1506 (s), 1384 (s), 1303 (s), 1034 (s) [ν(NO_3^-)], 3579 (m) [ν(NH)] cm^{-1}. $C_{15}H_{36}ErN_9O_{13}$ (716.76): calcd. C 25.1, H 5.1, N 17.6; found C 24.9, H 5.1, N 17.5.

[Tm(L)](NO$_3$)$_3$·5H$_2$O (12): Yield: 0.052 g (70%). MS (FAB): *m*/*z* = 585 $[TmL(NO_3)_2]^+$, 523 $[TmL(NO_3)]^+$, 461 $[TmL]^+$, 293 $[L + H]^+$. IR (KBr): $\tilde{\nu}$ = 1605 (m) [ν(C=C) and ν(C=N)$_{py}$], 1502 (s), 1384 (s), 1300 (s), 1020 (s) [ν(NO_3^-)] cm^{-1}. $C_{15}H_{38}N_9O_{14}Tm$ (737.45): calcd. C 23.8, H 5.3, N 16.7; found C 23.8, H 4.0, N 16.0.

[Yb(L)](NO$_3$)$_3$·12H$_2$O·CH$_3$CN (13). Yield: 0.063 g (69%). MS (FAB): *m*/*z* = 590 $[YbL(NO_3)_2]^+$, 528 $[YbL(NO_3)]^+$, 466 $[YbL]^+$, 293 $[L + H]^+$. IR (KBr): $\tilde{\nu}$ = 1608 (m) [ν(C=C) and ν(C=N)$_{py}$], 1462 (s), 1384 (s), 1300 (s), 1034 (s) [ν(NO_3^-)] cm^{-1}. $C_{17}H_{55}N_{10}O_{21}Yb$ (908.71): calcd. C 21.0, H 5.7, N 14.4; found C 21.0, H 5.5, N 14.9.

[Lu(L)](NO$_3$)$_3$·2H$_2$O·2CH$_3$CN (14): Yield: 0.066 g (85%). MS (FAB): *m*/*z* = 591 $[LuL(NO_3)_2]^+$, 529 $[LuL(NO_3)]^+$, 293 $[L + H]^+$. IR (KBr): $\tilde{\nu}$ = 1608 (m) [ν(C=C) and ν(C=N)$_{py}$], 1503 (m), 1384 (s), 1300 (m), 1050 (m) [ν(NO_3^-)], 3195 (m) [ν(NH)] cm^{-1}. $C_{19}H_{38}LuN_{11}O_{11}$ (771.22): calcd. C 29.6, H 5.0, N 20.0; found C 30.0, H 5.0, N 19.8. Crystals of formula $[Lu(L)(NO_3)_2](ClO_4)$ suitable for X-ray diffraction were obtained from the mother liquid.

Crystal Structure Determinations: By slow recrystallization of compounds **1**–**4** and from the mother liquid for **14**, crystals suitable for X-ray diffraction were obtained. The details on the X-ray crystal data, structure solution and refinement are given in Table 4. Measurements were made with a Bruker X8 Kappa APEX II for **2** and with a Bruker Smart-CCD-1000 for the remaining complexes. Graphite monochromated Mo-K_α was used. All data were corrected by Lorentz and polarization effects. Empirical absorption corrections were also applied.[36] Complex scattering factors were taken from the program package SHELX-97.[37] The structures were solved by direct methods by using SIR-92,[38] which revealed the position of all non-hydrogen atoms. All the structures were refined on F^2 by a full-matrix least-squares procedure by using anisotropic displacement parameters for all non-hydrogen atoms. The hydrogen atoms of the carbon atoms were located in their calculated positions and refined by using a riding model. The hydrogen atoms of the amine groups were located on a difference Fourier map and refined isotropically.

In crystals of **3**, the unit cell contains two potential solvent-accessible symmetry-related cavities, filled with disordered solvent, probably 1,4-dioxane. The volume of each cavity is 928 Å^3. Attempts to model dioxane molecules into the solvent density did not result in an acceptable model. As an alternative strategy, the SQUEEZE[39] function of PLATON[40] was used to eliminate the contribution of the electron density in the solvent region from the intensity data. The use of this strategy and the subsequent solvent-free model produced much better refinement results than the attempt to model the solvent atoms. Therefore, the solvent-free model and intensity data were used for the final results reported here. A total of 320 e was found in each cavity, corresponding to approximately six dioxane molecules per cavity. Where relevant, the crystal data reported earlier in this paper are given without the contribution of the disordered solvent. Molecular graphics were generated by using CAMERON[41] and ORTEP-3.[42]

CCDC-708226 (for **1**), -708227 (for **2**), -708225 (for **3**), -708224 (for **4**), and -708228 (for **14**) contain the supplementary crystallographic data for this paper. These data can be obtained free of charge from The Cambridge Crystallographic Data Centre via www.ccdc.cam.ac.uk/data_request/cif.

Computational Methods: All calculations were performed by employing hybrid DFT with the B3LYP exchange-correlation functional,[43,44] and the Gaussian 03 package (Revision C.01).[45] Different computational studies on Ln^{III} complexes have shown that the 4f orbitals do not participate in bonding because of their contraction into the core.[46] As a consequence, no effect of the spin-orbital coupling on the equilibrium geometries of Ln^{III} complexes was found.[47] Thus, spin-orbit effects were not taken into account in the present work. Relativistic effects were considered through the use of relativistic effective core potentials (RECP). Full geometry optimizations of the $[Ln(L)(NO_3)_3]$ and $[Ln(L)(NO_3)_2]^+$ systems (Ln = La, Pr, Nd, Gd, Ho, or Lu) systems were performed in vacuo by using the RECP of Dolg et al. and the related [5s4p3d]-GTO valence basis set for the lanthanides,[26] and the 6-31G(d) basis set for C, H, N and O atoms. The RECP of Dolg et al. includes 46+4f^n electrons in the core, leaving the outermost 11 electrons to be treated explicitly, in line with the nonparticipation of 4f electrons in bonding. Thus, this RECP treats [Kr]4d^{10}4f^n as fixed core for

Table 4. Crystal data and structure refinement for compounds **1**–**4** and **14**.

	1	**2**	**3**	**4**	**14**
Empirical formula	$C_{15}H_{30}LaN_9O_{10}$	$C_{15}H_{30}CeN_9O_{10}$	$C_{15}H_{28}N_9O_9Pr$	$C_{15}H_{30}N_9NdO_{10}$	$C_{15}H_{28}ClLuN_8O_{10}$
Molecular mass / g mol^{-1}	635.39	636.60	619.37	640.72	690.87
Crystal system	triclinic	triclinic	monoclinic	monoclinic	monoclinic
Space group	$P\bar{1}$	$P\bar{1}$	$P2_1/n$	$P2_1/n$	$P2_1/c$
a / Å	8.2819(14)	8.1898(2)	12.712(2)	16.819(3)	10.507(2)
b / Å	10.9365(19)	10.8730(3)	11.087(2)	8.7857(17)	9.607(2)
c / Å	14.134(2)	13.9478(4)	27.966(5)	16.851(3)	23.370(5)
α / °	90.692(3)	80.748(2)	–	–	–
β / °	107.017(3)	73.264(2)	101.773(3)	105.802(3)	91.564(4)
γ / °	104.551(3)	75.481(2)	–	–	–
V / Å^3	1179.8(3)	1146.16(5)	3858.7(12)	2395.9(8)	2358.2(9)
Z	2	2	4	4	4
$\rho_{calcd.}$ / g cm^{-3}	1.789	1.845	1.066	1.776	1.946
μ / mm^{-1}	1.880	2.058	1.302	2.236	4.368
R_{int}	0.0194	0.0392	0.0338	0.0291	0.1333
R_1[a]	0.0149	0.0146	0.0280	0.0215	0.0838
wR_2 (all data)[b]	0.0385	0.0356	0.0730	0.0573	0.2171

[a] $R_1 = \Sigma||F_o| - |F_c||/\Sigma|F_o|$. [b] $wR_2 = \{\Sigma[w(|F_o|^2 - |F_c|^2)^2]/\Sigma[w(F_o^4|)]\}^{1/2}$.

each lanthanide, whereas only the $5s^25p^66s^25d^16p^0$ shell is explicitly taken into account. In the case of the $[Ln(L)(NO_3)_3]$ systems the X-ray crystal structure of the La^{III} complex was used as input geometry, whereas for the $[Ln(L)(NO_3)_2]^+$ systems the solid-state structures of the Nd^{III} and Lu^{III} complexes were used as starting structures. The issue of whether the optimized geometries correspond to local or global minima on the potential energy surface was not addressed in the present work. The stationary points found on the potential energy surfaces as a result of the geometry optimizations were tested to represent energy minima rather than saddle points by frequency analysis.

In acetonitrile solution solvation energies and free energies of reaction were calculated from solvated single-point energy calculations on the geometries optimized in vacuo. Solvent effects were evaluated by using the polarizable continuum model (PCM). In particular, we used the C-PCM variant[48] that employs conductor rather than dielectric boundary conditions. The solute cavity is built as an envelope of spheres centered on atoms or atomic groups with appropriate radii. In our calculations we applied the united atom topological mode[49] on radii optimized for the PBE0/6-31G(d) level of theory. Calculations were performed by using an average area of 0.2 $Å^2$ for all the finite elements (tesserae) used to build the solute cavities. Final free energies of reaction include both electrostatic and nonelectrostatic contributions.

Supporting Information (see footnote on the first page of this article): Bond angles of the metal coordination environments and hydrogen-bonding data for compounds **1**–**4** and **14**; views of the X-ray crystal structures of the $[Ln(L)(NO_3)_3]$ complexes (Ln = Ce or Pr) and in vacuo optimized Cartesian coordinates for the $[Ln(L)(NO_3)_3]$ and $[Ln(L)(NO_3)_2]^+$ systems (Ln = La, Ce, Pr, Nd, Gd, Ho, or Lu).

Acknowledgments

We thank Xunta de Galicia (Spain) (Project PGIDIT07-PXIB209039PR) for financial support. The authors are indebted to the Centro de Supercomputación de Galicia (CESGA) for providing the computer facilities. We are also grateful to Unidade de Raios X, RIAIDT, University of Santiago de Compostela (Spain) for recording the X-ray intensity measurements. C.N. thanks Xunta de Galicia for her Maria Barbeito program predoctoral contract.

[1] a) R. B. Lauffer in *MRI Clinical Magnetic Resonance Imaging* (Eds.: R. R. Edelman, M. B. Zlatkin, J. R. Hesselink, W. B. Saunders), 2nd ed., Philadelphia, **1996**, vol. 1, ch. 5; b) P. Caravan, J. J. Ellinson, T. J. McMurry, R. B. Lauffer, *Chem. Rev.* **1999**, *99*, 2293–2352; c) A. E. Merbach, É. Tóth (Eds.), *The Chemistry of Contrast Agents in Medical Magnetic Resonance Imaging*, Wiley, New York, **2001**.
[2] I. Hemmilä, T. Stahlberg, P. Mottram (Eds.), *Bioanalytical Applications of Labelling Technologies*, Wallac Oy, Turku, **1994**.
[3] D. Parker, *Coord. Chem. Rev.* **2000**, *205*, 109–130.
[4] a) T. C. Bruice, A. Tsubouchi, R. O. Dempcy, L. P. Olson, *J. Am. Chem. Soc.* **1996**, *118*, 9867–9875; b) P. Hurst, B. K. Takasaki, J. Chin, *J. Am. Chem. Soc.* **1996**, *118*, 9982–9983.
[5] a) G. L. De Nardo, G. R. Mirik, L. A. Kroger, R. T. O'Donnel, C. F. Meares, S. L. De Nardo, *J. Nucl. Med.* **1996**, *37*, 451–456; b) M. J. Heeg, S. S. Jurisson, *Acc. Chem. Res.* **1999**, *32*, 1053–1060.
[6] a) J.-C. G. Bünzli in *Rare Earths* (Eds.: R. Saez-Puche, P. Caro), Editorial Complutense, Madrid, **1998**; b) D. Parker, R. S. Dickins, H. Puschmann, C. Crossland, J. A. K. Howard, *Chem. Rev.* **2002**, *102*, 1977–2010.
[7] V. Alexander, *Chem. Rev.* **1995**, *95*, 273–342.
[8] a) W. D. Kim, G. E. Kiefer, F. Maton, K. McMillan, R. N. Muller, A. D. Sherry, *Inorg. Chem.* **1995**, *34*, 2233–2243; b) S. Aime, M. Botta, L. Frullano, S. G. Crich, G. Giovenzana, R. Pagliarin, G. Palmisano, F. R. Sirtori, M. Sisti, *J. Med. Chem.* **2000**, *43*, 4017–4024; c) S. Aime, E. Gianolio, D. Corpillo, C. Cavallotti, G. Palmisano, M. Sisti, G. B. Giovenzana, R. Pagliarin, *Helv. Chim. Acta* **2003**, *86*, 615–632.
[9] J. Gregolinski, K. Slepokura, J. Lisowski, *Inorg. Chem.* **2007**, *46*, 7923–7934.
[10] L. Valencia, J. Martínez, A. Macías, R. Bastida, R. A. Carvalho, C. F. G. C. Geraldes, *Inorg. Chem.* **2002**, *41*, 5300–5312.
[11] a) M. del C. Fernández-Fernández, R. Bastida, A. Macías, P. Pérez-Lourido, C. Platas-Iglesias, L. Valencia, *Inorg. Chem.* **2006**, *45*, 4484–4496; b) C. Nuñez, R. Bastida, A. Macias, M. Mato-Iglesias, C. Platas-Iglesias, L. Valencia, *Dalton Trans.* **2008**, 3841–3850.
[12] S. W. A. Bligh, N. Choi, C. F. G. C. Geraldes, S. Knoke, M. McPartlin, M. J. Sanganee, T. M. Woodroffe, *J. Chem. Soc., Dalton Trans.* **1997**, 4119–4126.
[13] N. S. Gill, R. H. Nuttall, D. E. Scaife, D. W. A. Sharp, *J. Inorg. Nucl. Chem.* **1961**, *18*, 79–87.
[14] W. T. Carnall, S. Siegel, J. R. Ferraro, B. Tani, E. Gebert, *Inorg. Chem.* **1973**, *12*, 560–564.
[15] M. Seitz, A. G. Oliver, K. N. Raymond, *J. Am. Chem. Soc.* **2007**, *129*, 11153–11160.
[16] C. Platas, F. Avecilla, A. de Blas, T. Rodríguez-Blas, R. Bastida, A. Macías, A. Rodríguez, H. Adams, *J. Chem. Soc., Dalton Trans.* **2001**, 1699–1705.
[17] A. M. Arif, J. D. J. Backer-Dirks, C. J. Gray, F. A. Hart, M. B. Hursthouse, *J. Chem. Soc., Dalton Trans.* **1987**, 1665–1673.
[18] F. Benetollo, A. Polo, G. Bombieri, K. K. Fonda, L. M. Vallarino, *Polyhedron* **1990**, *9*, 1411–1422.
[19] J. L. Sessler, T. D. Mody, G. W. Hemmi, V. Lynch, *Inorg. Chem.* **1993**, *32*, 3175–3187.
[20] R. Rodríguez-Cortiñas, F. Avecilla, C. Platas-Iglesias, D. Imbert, J.-C. G. Bünzli, A. de Blas, T. Rodríguez-Blas, *Inorg. Chem.* **2002**, *41*, 5336–5349.
[21] a) C. A. Hunter, J. K. M. Sanders, *J. Am. Chem. Soc.* **1990**, *112*, 5525–5534; b) R.-F. Song, Y.-B. Xie, J.-R. Li, X.-H. Bu, *Dalton Trans.* **2003**, 4742–4748.
[22] R. K. Harris, *Nuclear Magnetic Resonance Spectroscopy: A Physicochemical view*, Pitman, London, **1983**.
[23] J. A. Peters, J. Huskens, D. J. Raber, *Prog. NMR Spectrosc.* **1996**, *28*, 283–350.
[24] S. Aime, L. Barbero, M. Botta, G. Ermondi, *J. Chem. Soc., Dalton Trans.* **1992**, 225–228.
[25] J. H. Forsberg, R. M. Delaney, Q. Zhao, G. Harakas, R. Chandran, *Inorg. Chem.* **1995**, *34*, 3705–3715.
[26] M. Dolg, H. Stoll, A. Savin, H. Preuss, *Theor. Chim. Acta* **1989**, *75*, 173–194.
[27] a) M. Gonzalez-Lorenzo, C. Platas-Iglesias, F. Avecilla, S. Faulkner, S. J. A. Pope, A. de Blas, T. Rodriguez-Blas, *Inorg. Chem.* **2005**, *44*, 4254–4262; b) M. Mato-Iglesias, A. Roca-Sabio, A. Pálinkás, D. Esteban-Gómez, C. Platas-Iglesias, E. Tóth, A. de Blas, T. Rodríguez-Blas, *Inorg. Chem.* **2008**, *47*, 7840–7851.
[28] U. Cosentino, A. Villa, D. Pitea, G. Moro, V. Barone, A. Maiocchi, *J. Am. Chem. Soc.* **2002**, *124*, 4901–4909.
[29] C. Platas-Iglesias, M. Mato-Iglesias, K. Djanashvili, R. N. Muller, L. Vander Elst, J. A. Peters, A. de Blas, T. Rodríguez-Blas, *Chem. Eur. J.* **2004**, *10*, 3579–3590.
[30] N. Quali, B. Bocquet, S. Rigault, P.-Y. Morgantini, J. Weber, C. Piguet, *Inorg. Chem.* **2002**, *41*, 1436–1445.
[31] M. Mato-Iglesias, E. Balogh, C. Platas-Iglesias, É. Tóth, A. de Blas, T. Rodríguez-Blas, *Dalton Trans.* **2006**, 5404–5415.
[32] a) M. R. Willcott, R. E. Lenkinski, R. E. Davis, *J. Am. Chem. Soc.* **1972**, *94*, 1742–1744; b) R. E. Davis, M. R. Willcott, *J. Am. Chem. Soc.* **1972**, *94*, 1744–1745.
[33] G. A. Shamov, G. Schreckenbach, R. L. Martin, P. J. Hay, *Inorg. Chem.* **2008**, *47*, 1465–1475.

[34] N. W. Alcock, R. G. Kingston, P. Moore, C. Pierpoint, *J. Chem. Soc., Dalton Trans.* **1984**, 1937–1943.
[35] G. L. Rothermel Jr, L. Miao, A. L. Hill, S. C. Jackels, *Inorg. Chem.* **1992**, *31*, 4854–4859.
[36] G. M. Sheldrick, *Sadabs: Program for Empirical Absorption Correction of Area Detector Data*, University of Göttingen, Germany, **1996**.
[37] G. M. Sheldrick, *SHELX-97: An Integrated System for Solving and Refining Crystal Structures from Diffraction Data*, University of Göttingen, Germany, **1997**.
[38] A. Altornare, G. Cascarano, C. Giacovazzo, A. Gualardi, *J. Appl. Crystallogr.* **1993**, *26*, 343–350.
[39] P. Sluis, A. L. van der Spek, *Acta Crystallogr., Sect. A* **1990**, *46*, 194–201.
[40] A. L. Spek, *PLATON*, University of Utrecht, The Netherlands, **2001**.
[41] D. M. Watkin, L. Pearce and C. K. Prout, *CAMERON: A Molecular Graphics Package*, Chemical Crystallography Laboratory, University of Oxford, England, **1993**.
[42] ortep-3: L. J. Farrugia, *J. Appl. Crystallogr.* **1997**, *30*, 565.
[43] A. D. Becke, *J. Chem. Phys.* **1993**, *98*, 5648–5652.
[44] C. Lee, W. Yang, R. G. Parr, *Phys. Rev. B* **1988**, *37*, 785–789.
[45] M. J. Frisch, G. W. Trucks, H. B. Schlegel, G. E. Scuseria, M. A. Robb, J. R. Cheeseman, J. A. Montgomery Jr, T. Vreven, K. N. Kudin, J. C. Burant, J. M. Millam, S. S. Iyengar, J. Tomasi, V. Barone, B. Mennucci, M. Cossi, G. Scalmani, N. Rega, G. A. Petersson, H. Nakatsuji, M. Hada, M. Ehara, K. Toyota, R. Fukuda, J. Hasegawa, M. Ishida, T. Nakajima, Y. Honda, O. Kitao, H. Nakai, M. Klene, X. Li, J. E. Knox, H. P. Hratchian, J. B. Cross, V. Bakken, C. Adamo, J. Jaramillo, R. Gomperts, R. E. Stratmann, O. Yazyev, A. J. Austin, R. Cammi, C. Pomelli, J. W. Ochterski, P. Y. Ayala, K. Morokuma, G. A. Voth, P. Salvador, J. J. Dannenberg, V. G. Zakrzewski, S. Dapprich, A. D. Daniels, M. C. Strain, O. Farkas, D. K. Malick, A. D. Rabuck, K. Raghavachari, J. B. Foresman, J. V. Ortiz, Q. Cui, A. G. Baboul, S. Clifford, J. Cioslowski, B. B. Stefanov, G. Liu, A. Liashenko, P. Piskorz, I. Komaromi, R. L. Martin, D. J. Fox, T. Keith, M. A. Al-Laham, C. Y. Peng, A. Nanayakkara, M. Challacombe, P. M. W. Gill, B. Johnson, W. Chen, M. W. Wong, C. Gonzalez, J. A. Pople, *Gaussian 03*, Revision C.01, Gaussian, Inc., Wallingford, CT, **2004**.
[46] a) L. Maron, O. Eisenstein, *J. Phys. Chem. A* **2000**, *104*, 7140–7143; b) C. Boehme, B. Coupez, G. Wipff, *J. Phys. Chem. A* **2002**, *106*, 6487–6498.
[47] V. Vetere, P. Maldivi, C. Adamo, *J. Comput. Chem.* **2003**, *24*, 850–858.
[48] V. Barone, M. Cossi, *J. Phys. Chem. A* **1998**, *102*, 1995–2001.
[49] V. Barone, M. Cossi, J. Tomasi, *J. Chem. Phys.* **1997**, *107*, 3210–3221.

Received: November 6, 2008
Published Online: February 2, 2009

